Soft Matter

PAPER

View Article Online
View Journal | View Issue

Cite this: *Soft Matter*, 2018, **14**, 945

Activity-induced instability of phonons in 1D microfluidic crystals†

Alan Cheng Hou Tsang,[ab] Michael J. Shelley[cd] and Eva Kanso *[acd]

One-dimensional crystals of passively-driven particles in microfluidic channels exhibit collective vibrational modes reminiscent of acoustic 'phonons'. These phonons are induced by the long-range hydrodynamic interactions among the particles and are neutrally stable at the linear level. Here, we analyze the effect of particle activity – self-propulsion – on the emergence and stability of these phonons. We show that the direction of wave propagation in active crystals is sensitive to the intensity of the background flow. We also show that activity couples, at the linear level, transverse waves to the particles' rotational motion, inducing a new mode of instability that persists in the limit of large background flow, or, equivalently, vanishingly small activity. We then report a new phenomenon of phonons switching back and forth between two adjacent crystals in both passively-driven and active systems, similar in nature to the wave switching observed in quantum mechanics, optical communication, and density stratified fluids. These findings could have implications for the design of commercial microfluidic systems and the self-assembly of passive and active micro-particles into one-dimensional structures.

Received 5th July 2017,
Accepted 28th December 2017

DOI: 10.1039/c7sm01335c

rsc.li/soft-matter-journal

1 Introduction

The ability to manipulate and organize the collective motion of droplets and particles in microfluidic channels is relevant to numerous applications in physics and biology. Examples include the pharmaceutical and food industries,[1,2] lab-on-a-chip applications,[1] and the control and self-assembly of passive and active colloids.[3–6] The latter is particularly attractive as a new paradigm for the fabrication of modular materials, such as one-dimensional (1D) active structures, and for advancing the field of active systems beyond the classical study of particle suspensions.[7–9]

A striking phenomenon in 1D lattices of passively-driven droplets is the propagation of waves, or phonons, due to hydrodynamic interactions (HIs) among the droplets.[10–13] Similar waves are observed in arrays of particles in optical traps.[14,15] Phonons in these passively-driven systems are neutrally stable and exhibit nonlinear instabilities due to mode coupling.[16–18]

Understanding wave instabilities in microfluidic systems is particularly important for the self-assembly and rearrangement of particles into 1D structures.[19,20] In this study, we analytically and computationally analyze the effect of activity on the stability of 1D lattices of particles confined in microfluidic channels (see Fig. 1(a)). We show that activity induces a new mode of wave instability at the linear level that arises from the coupling between the translational and rotational motion of the particles. The rate of growth of this instability can be controlled by varying the intensity of the background flow. Importantly, active lattices exhibit singular behavior in the sense that this instability persists in the limit of vanishingly small activity. We then report back-and forth switching of waves between adjacent 1D lattices of active and passively-driven particles, reminiscent in nature to the wave switching observed in many other systems such as in quantum, optical and stratified flow physics.

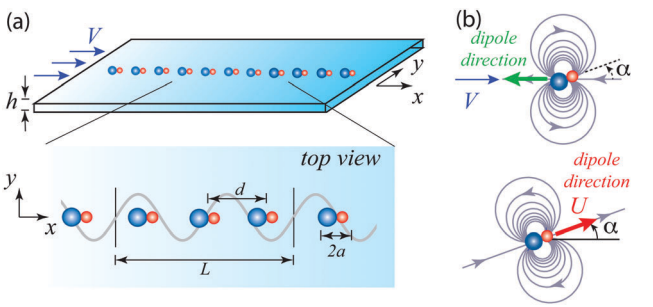

Fig. 1 (a) Particles confined in a microfluidic flow channel. (b) Dipolar far-field flows induced by the background flow (top) and the particle self-propelled motion (bottom).

[a] *Aerospace and Mechanical Engineering, University of Southern California, Los Angeles, California 90089, USA. E-mail: kanso@usc.edu*
[b] *Bioengineering, Stanford University, Stanford, California 94305, USA*
[c] *Center for Computational Biology, Flatiron Institute, New York, New York 10010, USA*
[d] *Courant Institute of Mathematical Sciences, New York University, New York, New York 10012, USA*

† Electronic supplementary information (ESI) available. See DOI: 10.1039/c7sm01335c

2 Model

We consider a system of particles, each is a dumbbell with small ''head'' and large ''tail'', confined in a Hele-Shaw flow channel of height h. The 2D height-averaged flow is irrotational.[21–23] Potential flow theory can thus be applied to study the interactions of particles in the unconfined complex plane $z = x + iy$; see Fig. 1(a). Indeed, one can rigorously prove that the leading order term in the far-field expansion of the velocity field produced by a moving particle in confinement corresponds to a potential dipole in the (x, y) plane; see Section 1 of the ESI.† [24] The fact that the flow is dipolar is independent of the details of the particle transport mechanism, passively-driven or self-propelled.[10,13,25–27] Mathematically, the complex conjugate of the velocity field $\omega(z)$ created by particle n, located at z_n with orientation α_n relative to the x-axis, can be written as $\bar{\omega}(z) = \sigma_n/(z - z_n)^2$, where σ_n is the dipole strength. For active particles, σ_n depends on the particle's swimming speed U and orientation α_n; for passive particles, the dipole strength σ_n is a function of the driving flow direction and not of the particle orientation (Fig. 1b).

The translational motion of an active particle at z_n is due to its self-propulsion at speed U in the (x, y) plane and to advection by the uniform background flow V and the dipolar flow disturbance created by all other particles. This advection speed depends on the particle's geometric properties, represented by the lumped motility coefficient μ, where $0 < \mu < 1$. Due to confinement, the particle's orientation α_n changes in response to the local flow at z_n created by the background flow V and all other particles. This response is scaled by a rotational motility coefficient ν. Large tail particles for which ν is positive tend to align with the local flow, whereas large head particles for which ν is negative tend to align opposite to the local flow.[27,28] In this work, we analyze the stability of downstream motion for large tail particles in flow channels; large head particles will always align upstream. To this end, the governing equations are given by (see ref. 28–30 and Section 2 of the ESI† [24] for more details)

$$\begin{aligned} \dot{\bar{z}}_n &= U e^{-i\alpha_n} + \mu\left(V + \sum_{m\neq n} \frac{\sigma_m}{(z_n - z_m)^2}\right), \\ \dot{\alpha}_n &= \nu \mathrm{Real}\left[ie^{i\alpha_n}\left(V + \sum_{m\neq n} \frac{\sigma_m}{(z_n - z_m)^2}\right)\right]. \end{aligned} \tag{1}$$

The strength σ_m of the dipolar disturbance created by the mth particle due to its self-propelled motion U and the background flow V is given by

$$\sigma_m = a^2 U e^{i\alpha_m} - a^2(1 - \mu)V. \tag{2}$$

Here, a represents an effective radius of the confined particle in the (x, y) plane; a is the radius of a circular cylinder that creates a dipolar flow equivalent in the far field to that of the confined particle (see Section 1 of the ESI† [24]).

To numerically investigate the dynamics of the infinite system of particles in (1), it is convenient to represent it using N particles in a periodic domain of size L; see Fig. 1(a). The HIs between particles give rise to a bi-infinite sum which we rewrite in closed-form as

$$\bar{\omega} = \sum_{\substack{m=-\infty \\ m\neq n}}^{\infty} \frac{\sigma_m}{(z_n - z_m)^2} = \frac{\pi^2}{L^2} \sum_{\substack{m=1 \\ m\neq n}}^{N} \sigma_m \csc^2\left[\frac{\pi}{L}(z_n - z_m)\right]. \tag{3}$$

Eqn (1)–(3) form a closed-system that we use to solve for the propagation of phonons in a 1D lattice of active particles.

Passive particles ($U = 0$) are a special case of (1)–(3) for which the translation and orientation equations are decoupled at the leading order in velocity even for non-spherical particles.[27] This decoupling is rooted in the fact that the strength σ_m of the dipolar far-field flow depends on the direction of the driving flow and not on α_m. Therefore, for passive particles, it is sufficient to consider the translational equations in (1); see ref. 10 and 13.

3 Results and discussion

1D active crystal

The 1D crystal lattice configuration satisfies $z_{n+1} - z_n = d$ and $\alpha_n = 0$ with constant spacing d between neighboring particles ($d > 2a$). This configuration is an equilibrium solution of (1)–(3): all particles have zero rotational velocity $\dot{\alpha}_{\mathrm{lattice}} = 0$ and constant translational velocity $\dot{\bar{z}}_{\mathrm{lattice}} = U + \mu(V + u)$. Here, $u = \pi^2\sigma/3d^2$ is the velocity arising from HIs among the particles and $\sigma = a^2[U - (1 - \mu)V]$ is the dipole strength. In a dilute suspension, the velocity of active particles is $U_{\mathrm{dilute}} = U + \mu V$ (see ref. 30). HIs can speed up or slow down the particles relative to U_{dilute}, depending on the strength of the background flow V. This is because V influences the dipolar flow disturbance created by the particles: for $V > U_{\mathrm{dilute}}$, the dipole strength σ is negative and the dipolar flow points opposite to the driving flow (see top schematic of Fig. 1b) producing negative u and slowing down the lattice in comparison with the speed of a particle in a dilute channel. If we tune the background flow properly such that $V = U_{\mathrm{dilute}}$, the components of the dipole strength due to self-propulsion and background flow cancel out; HIs are suppressed ($u = \sigma = 0$) and the lattice velocity is equal to U_{dilute}. For $V < U_{\mathrm{dilute}}$, both σ and u are positive, increasing the speed of each particle in the lattice. Therefore, the lattice moves faster for weak flows $V < U_{\mathrm{dilute}}$ and slower for strong flows $V > U_{\mathrm{dilute}}$. This non-monotonic dependence of lattice velocity on the speed V of the background flow is unique to active crystals; for passive particles, the lattice velocity is given by $\mu(V + u)$ and is always smaller than the particle velocity μV in a dilute suspension.[10] In both active and passive crystals, closely-spaced lattices with smaller d induce stronger HIs and, thus, larger magnitudes of u and faster motions relative to the dilute suspension – an effect referred to as the 'peloton effect' due to collective drag reduction in ref. 10.

Nonlinear behavior of active phonons

We examine the stability of active lattices to small perturbations in position and orientation $z_n \equiv z_n|_{\mathrm{lattice}} + \delta z_n$ and $\alpha_n \equiv \delta\alpha_n$, where $(\delta z_n, \delta\alpha_n)$ evolve in the lattice frame of reference.

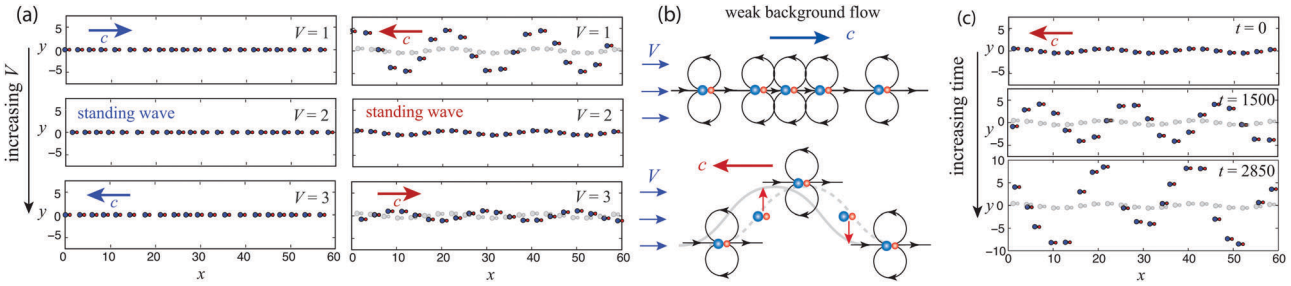

Fig. 2 Active particles: (a) snapshots of the longitudinal and transverse modes for $U = 1$, $k = 3\pi/10$ and different background flow velocity $V = 1$, 2 and 3 at $t = 2000$. The arrows indicate the directions of wave propagation. Initial perturbation is superimposed in grey to highlight the growth in the transverse mode. (b) Schematic depicting hydrodynamic-interactions among neighboring particles for $V < U_{\text{dilute}}$. (c) Details of the slowly growing transverse mode for $V = 1$. See the ESI,† Movies 3 and 4. In all cases, $\mu = 0.5$, $\nu = 1$.

We particularly consider longitudinal and transverse wave perturbations of the form $\delta z_n = X_n = Ae^{j(knd-\omega t)}$ and $\delta z_n = iY_n = iBe^{j(knd-\omega t)}$. Here, k is the perturbation wavenumber, ω the perturbation frequency, j the complex unit in the wave plane ($j^2 = -1$). The amplitudes A and B are taken to be small compared to the inter-particle distance d. The perturbations in particle orientation $\delta\alpha_n = \Theta_n$ are initially zero.

We first numerically evolve the nonlinear, coupled translational and rotational eqn (1), using (3), for an infinite active lattice with periodicity L subject to wave perturbations. To this end, we give the system an initial perturbation away from the lattice configuration in the form of a sinusoidal wave with wavelength $2\pi/k$. To obtain the desired value of k, we vary the number of particles N and the domain length L while keeping L an integer multiple of the initial lattice spacing d to ensure periodic boundary conditions. Additional details on the numerical implementation are given in Section 6 of the ESI.†[24] The direction of wave propagation depends on the background flow V, which in turn dictates the sign of the dipolar strength σ (see Fig. 2(a)). For a weak background flow ($V < U_{\text{dilute}}$) such that the dipole strength is positive ($\sigma > 0$), longitudinal waves X_n propagate downstream and transverse waves Y_n move upstream, in opposite directions to their counterparts in passively-driven lattices. If we tune the background flow properly ($V = U_{\text{dilute}}$) such that $\sigma = u = 0$, we obtain standing waves. For strong background flows ($V > U_{\text{dilute}}$) such that $\sigma < 0$, the waves propagate similarly to passive lattices. This change in wave direction can be explained intuitively based on the HIs among the particles. When the background flow is weak, $\sigma > 0$ and HIs cause a longitudinally-dense pack of particles to move faster than other particles in the lattice, thus traveling with the background flow (see top schematic of Fig. 2b). Meanwhile, HIs push transversally-deflected particles in opposite directions such that the transverse wave travels opposite to the flow (see bottom schematic of Fig. 2b). The opposite effect is obtained when the background flow is dominant, including the passive case $U = 0$. Fig. 2(a) indicates that the longitudinal waves X_n are stable while the transverse waves Y_n grow in time (see the ESI,† Movies 3 and 4) and that the growth rate of the transverse waves depends on V. Fig. 2(c) shows snapshots depicting the growth in wave amplitude over time. In contrast, passively-driven lattices ($U = 0$) exhibit stable longitudinal and transverse waves similar to those observed experimentally in arrays of microfluidic droplets[10] (see Movies 1 and 2, ESI†).

Linear stability analysis

We now analyze the lattice stability by linearizing (1) about the uniform lattice configuration. In the linear equations, HIs give rise to an infinite sum of the form $\sum_{m=-\infty}^{\infty} 2\sigma(\delta z_n - \delta z_m)/(md)^3$, for which we derive an exact expression for plane-wave solutions (see the ESI†[24]). We obtain $\sum_{m=-\infty}^{\infty} 2\sigma(\delta z_n - \delta z_m)/(md)^3 = j\delta z_n\Omega$, where

$$\Omega = \frac{2\sigma}{d^3}\left[\frac{\pi^2}{3}(kd) - \frac{\pi}{2}(kd)^2\text{sgn}(k) + \frac{1}{6}(kd)^3\right], \tag{4}$$

and sgn(·) denotes the signum function. By virtue of (4), recalling that $\delta z_n = X_n + iY_n$ and $\delta\alpha_n = \Theta_n$, the linear equations of motion can be written in matrix form as

$$\begin{pmatrix} \dot{X}_n \\ \dot{Y}_n \\ \dot{\Theta}_n \end{pmatrix} = \left(\begin{array}{c|cc} -j\mu\Omega & 0 & 0 \\ \hline 0 & j\mu\Omega & U \\ 0 & j\nu\Omega & -\nu\tilde{V} \end{array}\right) \begin{pmatrix} X_n \\ Y_n \\ \Theta_n \end{pmatrix}, \tag{5}$$

where $\tilde{V} = V + u$. For $U \neq 0$, the transverse and orientational dynamics are coupled at the linear level and are decoupled from the longitudinal dynamics. To obtain analytic expressions for the wave dispersion relation $\omega(k)$, we solve (5) explicitly for all physically relevant wavenumbers k ($k \leq \pi/d$). For longitudinal waves X_n, the dispersion relation is given by $\omega = \mu\Omega$ for both active and passive particles. The dispersion relation $\omega(k)$ is real-valued for all k, indicating no growth in wave amplitudes over time. Thus, longitudinal waves are linearly stable for all k. For transverse waves Y_n, the dispersion relation $\omega(k)$ is given by (see the ESI†[24])

$$2\omega = -(\nu\tilde{V}j + \mu\Omega) \pm \sqrt{(\nu\tilde{V}j - \mu\Omega)^2 - 4\nu U\Omega j}. \tag{6}$$

Here, for active particles (non-zero U), one branch is a rapidly decaying stable solution ($\text{Im}[\omega] < 0$) and one branch is a growing unstable solution ($\text{Im}[\omega] > 0$) for all wavenumbers k. Thus, transverse waves are always unstable. For passive particles ($U = 0$), the two branches collapse to $\omega = -\mu\Omega$, indicating a neutrally-stable transverse mode consistent with the results in ref. 10.

Activity-induced instability in linear and nonlinear analysis

Fig. 3(a) and (b) show the dispersion relation Real[ω] and phase velocity c = Real[ω]/k for both longitudinal and transverse modes for various values of V. Analytical solutions of (5) are depicted in solid lines while the '×' symbols are estimated from our simulations of (1). Blue and red colors are used to distinguish between longitudinal and transverse solutions, respectively. The two modes travel in opposite directions dictated by the intensity of the background flow V, as noted earlier. However, transverse waves travel faster than longitudinal waves for all k and V, except for $V = U_{\text{dilute}}$ which results in standing waves. Fig. 3(c) shows the growth rate of the transverse wave for increasing values of V from $V = 1$ to $V \to \infty$. The growth rate of the instability is non-monotonic in V. For $V < U_{\text{dilute}}$ and $\sigma > 0$, an increase in V decreases the growth rate of the instability. This result is intuitive. Increasing V suppresses the orientation dynamics and reduces the effective dipole strength σ. Both effects suppress the instability. At $V = U_{\text{dilute}}$ and $\sigma = 0$, the growth rate is identically zero, indicating that in the absence of hydrodynamic interactions, the transverse (standing) wave is linearly stable. As V increases past U_{dilute}, the growth rate increases monotonically with V. This is counterintuitive as one expects strong background flows to suppress the orientation dynamics and, thus, the instability. But for $V > U_{\text{dilute}}$, increasing V results in an increase in the magnitude of σ, thereby leading to stronger hydrodynamic interactions among the particles and thus an increase in the growth rate. Interestingly, in the limit $V/U \to \infty$, the growth rate becomes independent of V as discussed next.

Persistent instability in the limit of vanishingly-small activity

As $V/U \to \infty$, the dipole strength σ, and consequently u and Ω, are proportional to V. It is thus convenient to write $\tilde{V} = VP$, where $P = 1 - \pi^2(1 - \mu)/3d^2$ is a positive parameter, and $\Omega = VQ(k)$, where $Q(k)$ is independent of V. We substitute back into (6) to get an explicit expression for the unstable branch of ω as $V/U \to \infty$, or equivalently as $U/V \to 0$,

$$\omega_\infty = -\mu VQ + j\frac{\nu\mu UQ^2}{(\nu^2 P^2 + \mu^2 Q^2)}. \tag{7}$$

Here, the dispersion relation Real[ω_∞] = $-\mu VQ$ = $-\mu\Omega$ is unbounded. This expression takes the same form as in the case $U/V = 0$. In contrast, the growth rate Im[ω_∞] of transverse perturbations is bounded and the limit is independent of V (see Fig. 3(d)). More importantly, this result shows that the limit $V/U \to \infty$, or equivalently $U/V \to 0$, is singular in the sense that it does not converge to the case $U/V = 0$. That is to say, the limit as the system approaches a passively-driven lattice is not equivalent to the case of a passively-driven lattice. This singular behavior arises from the fact that activity, no matter how small, causes the transverse and rotational motion of the particles to couple at the linear level, as manifested in (5). This coupling is not present in passively-driven lattices, which are linearly stable and exhibit only nonlinear instabilities.[10]

Switching of phonons in two trains of 1D crystals

We now examine the robustness of the passive and active 1D crystals to interactions with neighboring 1D crystals, which we call trains hereafter. We find that the HIs between two adjacent trains separated by a distance b couple the longitudinal and transverse modes, eventually destabilizing both modes in passively-driven and active trains (see the ESI†[24] and Movies 5–8). The instability arises at the nonlinear level in passive trains and at

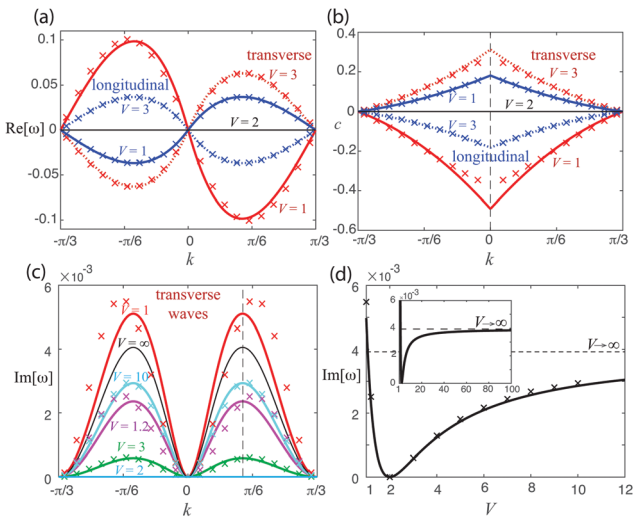

Fig. 3 Active particles: (a) dispersion relation and (b) phase velocity as a function of wavenumber k of longitudinal and transverse modes for V = 1, 2, and 3. The blue and red lines correspond to the longitudinal and transverse solutions respectively. The solid line is obtained analytically. The '×' markers denotes the numerical solutions. For all cases, U = 1, μ = 0.5, ν = 1. For $V = U_{\text{dilute}}$ = 2, one has ω = 0. (c) Growth rate *versus* k for V = 1, 1.2, 2, 3, 10, ∞, and (d) *versus* V for k = 0.5.

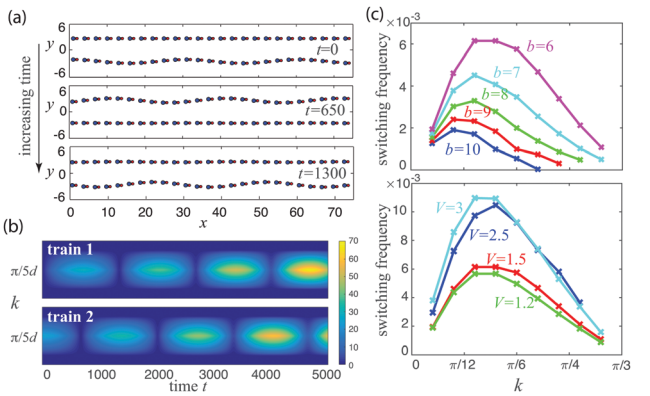

Fig. 4 (a) Phonons switching between two active trains; train 1 has no wave initially and train 2 has an initial wave of $k = \pi/(5d)$, U = 1, V = 1.5, b = 6. (b) Spatial Fourier spectrum *versus* time showing the switching in (a). The spectrum width is 0.06. The spectrum intensity given by the color bar is proportional to the wave amplitudes of the two trains, and the location of the peak of the spectrum shows the wave number. The wave amplitude of the two trains oscillates periodically and grows in time due to linear instability. The wave amplitude in one train reaches its maximum when the wave in the other train disappears, featuring the switching phenomenon. (c) Switching frequency as a function of wavenumber k for various separation distance b (top) and background flow V (bottom), where V is fixed at 1.5 for the cases shown on top, and b is fixed at 6 for the cases shown at the bottom. In all cases, μ = 0.5, ν = 1.

the linear level in active trains. At time scales shorter than the instability time scale, we observe switching of phonons between the two trains. Fig. 4 depicts the switching phenomenon for two active trains subject to initially small transverse perturbations in one train. The wave in one train induces a wave at about $\pi/2$ phase difference in the other train and *vice versa*. The switching frequency increases with decreasing inter-train distance b and increasing background flow V. This switching behavior is reminiscent of the well-known Rabi oscillations in multi-level quantum system,[31] switching of optical waves in two-core optical fibers[32] and of internal waves in two-layer density stratified fluids.[33] In these systems, the switching behavior is triggered by coupling due to wave resonance or nonlinearity. The present microfluidic system offers a new paradigm of wave switching due to nonlinear long-range HIs in Stokes flow. This phenomenon opens the door to exploring wave–wave interactions at low Reynolds numbers and, in the continuum limit, could have implications on understanding the synchronization of passive and active filaments in microchannels; see, *e.g.*, ref. 34–36.

4 Conclusions

We presented a first-principles theory of 1D crystals of active and passively-driven particles confined in microfluidic flow channels. We focused on elucidating the physical mechanisms underlying wave propagation in these crystals and the wave dependence on the particles' motility properties and intensity of the background flow. This theory can be exploited to devise novel processes for controlling the shape of the particle crystals. We showed that by properly tuning V, one can control the growth rate of the wave amplitude and even engineer a standing wave to ''freeze'' the lattice at any desired configuration. This is particularly useful for the self-assembly and fabrication of 1D structures and chains of various shapes and geometric properties. Another compelling scenario is to harness hydrodynamic interactions between trains of particles to control and rearrange particles within one train by direct manipulation of the other train. Finally, this theory can also serve as a design tool for predicting the parameters of high-throughput microfluidic channels when HIs between particles and trains of particles are not desirable.

Conflicts of interest

There are no conflicts to declare.

Acknowledgements

The work of E. Kanso is partially supported by the NSF INSPIRE grant 170731.

References

1 C. N. Baroud, F. Gallaire and R. Dangla, *Lab Chip*, 2010, **10**, 2032–2045.
2 A. S. Utada, E. Lorenceau, D. R. Link, P. D. Kaplan, H. A. Stone and D. A. Weitz, *Science*, 2005, **308**, 537–541.
3 W. Lee, H. Amini, H. A. Stone and D. D. Carlo, *Proc. Natl. Acad. Sci. U. S. A.*, 2010, **107**, 22413–22418.
4 W. E. Uspal and P. S. Doyle, *Soft Matter*, 2014, **10**, 5177–5191.
5 J. Zhang, E. Luijten and S. Granick, *Annu. Rev. Phys. Chem.*, 2015, **66**, 581–600.
6 M. S. D. Wykes, J. Palacci, T. Adachi, L. Ristroph, X. Zhong, M. D. Ward, J. Zhang and M. J. Shelley, *Soft Matter*, 2016, **12**, 4584–4589.
7 J. Dunkel, S. Heidenreich, K. Drescher, H. H. Wensink, M. Bär and R. E. Goldstein, *Phys. Rev. Lett.*, 2013, **110**, 228102.
8 D. Saintillan and M. J. Shelley, *C. R. Phys.*, 2013, **14**, 497–517.
9 M. C. Marchetti, J. F. Joanny, S. Ramaswamy, T. B. Liverpool, J. Prost, M. Rao and R. A. Simha, *Rev. Mod. Phys.*, 2013, **85**, 1143.
10 T. Beatus, T. Tlusty and R. Bar-Ziv, *Nat. Phys.*, 2006, **2**, 743–748.
11 T. Beatus, R. Bar-Ziv and T. Tlusty, *Phys. Rev. Lett.*, 2007, **99**, 124502.
12 M. Baron, J. Bławzdziewicz and E. Wajnryb, *Phys. Rev. Lett.*, 2008, **100**, 174502.
13 T. Beatus, R. H. Bar-Ziv and T. Tlusty, *Phys. Rep.*, 2012, **516**, 103–145.
14 G. M. Cicuta, J. Kotar, A. T. Brown, J.-H. Noh and P. Cicuta, *Phys. Rev. E: Stat., Nonlinear, Soft Matter Phys.*, 2010, **81**, 051403.
15 H. Nagar and Y. Roichman, *Phys. Rev. E: Stat., Nonlinear, Soft Matter Phys.*, 2014, **90**, 042302.
16 B. Liu, J. Goree and Y. Feng, *Phys. Rev. E: Stat., Nonlinear, Soft Matter Phys.*, 2012, **86**, 046309.
17 J.-B. Fleury, U. D. Schiller, S. Thutupalli, G. Gompper and R. Seemann, *New J. Phys.*, 2014, **16**, 063029.
18 U. D. Schiller, J.-B. Fleury, R. Seemann and G. Gompper, *Soft Matter*, 2015, **11**, 5850–5861.
19 J.-P. Raven and P. Marmottant, *Phys. Rev. Lett.*, 2009, **102**, 084501.
20 P. J. A. Janssen, M. D. Baron, P. D. Anderson, J. Blawzdziewicz, M. Loewenberg and E. Wajnryb, *Soft Matter*, 2012, **8**, 7495–7506.
21 G. Stokes, *Br. Assoc. Adv. Sci., Rep.*, 1898, **143**, 278.
22 H. Lamb, *Hydrodynamics*, Cambridge university press, 1932.
23 G. Taylor and P. Saffman, *Q. J. Mech. Appl. Math.*, 1959, **12**, 265–279.
24 See ESI,† for details.
25 T. Beatus, T. Tlusty and R. Bar-Ziv, *Phys. Rev. Lett.*, 2009, **103**, 114502.
26 N. Desreumaux, N. Florent, E. Lauga and D. Bartolo, *Eur. Phys. J. E: Soft Matter Biol. Phys.*, 2012, **35**, 1–11.
27 T. Brotto, J.-B. Caussin, E. Lauga and D. Bartolo, *Phys. Rev. Lett.*, 2013, **110**, 038101.
28 A. C. H. Tsang and E. Kanso, *Phys. Rev. E: Stat., Nonlinear, Soft Matter Phys.*, 2014, **90**, 021001.

29 A. C. H. Tsang and E. Kanso, *Phys. Rev. E: Stat., Nonlinear, Soft Matter Phys.*, 2015, **91**, 043008.
30 A. C. H. Tsang and E. Kanso, *Phys. Rev. Lett.*, 2016, **116**, 048101.
31 I. Rabi, *Phys. Rev.*, 1936, **49**, 324.
32 S. M. Jensen, *IEEE Trans. Microwave Theory Tech.*, 1982, **10**, 1568–1571.
33 M.-R. Alam, *Phys. Rev. Lett.*, 2012, **108**, 084502.
34 R. E. Goldstein, E. Lauga, A. I. Pesci and M. R. Proctor, *Phys. Rev. Fluids*, 2016, **1**, 073201.
35 E. Lauga and T. R. Powers, *Rep. Prog. Phys.*, 2009, **72**, 096601.
36 G. J. Elfring and E. Lauga, *J. Fluid Mech.*, 2011, **674**, 163–173.